Ab initio investigations on Sb_4 analogous Zintl clusters

F. Hagelberg, Sudha Srinivas, N. Sahoo, and T. P. Das
Department of Physics, State University of New York at Albany, Albany, New York 12222

K. G. Weil
Department of Materials Science and Engineering, The Pennsylvania State University, University Park, Pennsylvania 16802
(Received 12 September 1994; revised manuscript received 2 August 1995)

The validity of the Zintl-Klemm-Busmann (ZKB) principle is examined for the cluster series Sb_3SnA, Sb_3InA_2 (A=alkali-metal atom) and $Sb_3TeHalo$ (Halo=halogen atom), which have been recently discovered by Knudsen effusion mass spectrometry. In the Zintl anion systems Sb_3SnA and Sb_3InA_2, the alkali-metal atoms function, according to the ZKB principle, as electron donors. Since sizable electron transfer occurs from the alkali-metal-atom system to the Sb_3Sn or Sb_3In cluster nuclei, these units approach a 20-valence-electron configuration and therefore tetrahedral symmetry. From our *ab initio* treatment of the systems Sb_3SnA and Sb_3InA_2 with A=Na, K, or Cs it turns out that for both types of Zintl clusters a geometry is energetically favored which allows for maximal electron transfer and thereby for the closest possible approximation to tetrahedral symmetry of the cluster nuclei. This finding confirms that the ZKB principle is applicable to free clusters. For the Zintl cationic system $Sb_3TeHalo$ (Halo=Cl,Br,I), again a clear correspondence between electron transfer and cluster nucleus geometry is observed, but in contrast to the Zintl anion systems discussed in this work, the tetrahedral structure of the cluster nucleus does not turn out to be the stablest one. Quantitative comparisons between theoretical and measured ionization energies yield excellent agreement.

PACS number(s): 36.40.−c, 31.15.Ar, 33.15.Ry, 33.15.Ta

I. INTRODUCTION

The concept ''Zintl phase'' is traditionally applied to intermetallic compounds which exhibit a strongly polar bonding component [1,2]. According to the definition given by Zintl, Klemm, and Busmann [3], the term is understood in a narrower sense, involving the formation of an anionic sublattice in an intermetallic system. More specifically, the Zintl-Klemm-Busmann (ZKB) principle pertains to elements with valence electron number N whose structure remains unchanged if some of their atoms are replaced by an element with valence electron number $N-M$ and the missing M electrons are supplied by the addition of alkali-metal atoms. This rule is exemplified by the structure of the NaTl compound which is diamondlike. Due to electron transfer from the Na atom to the Tl atom, the third-group element Tl acquires the stoichiometry of the fourth-group element carbon. According to the ZKB principle, elemental identity determines the electronic properties of a Zintl phase much less than valence electron configuration. Thus, isoelectronic substitution, which changes a neutral into an anionic constituent, leaves the lattice structure invariant.

The ZKB principle has been applied very successfully to a large number of solid or liquid systems [2]. However, the discovery of ''Zintl clusters,'' occurring in the gaseous phase, has been reported only recently [3–7]. While a number of experimental structure determinations have been carried out on Zintl complexes in the liquid state stabilized by polar solvents [8], no such structural results are available in the case of Zintl clusters which have been detected in the vapor over solid or liquid intermediate mixtures [6,7]. These cluster species have been isolated only in such minute quantities that a direct observation of their structures would be difficult to carry out experimentally [12]. A theoretical *ab initio* treatment of these units, related to their geometries and electronic properties, is therefore of great current interest. In this work, we attempt such an exploration on three classes of spectroscopically detected Zintl clusters, two types of anionic species, and a cationic species.

We have focused our attention on Sb-based Zintl clusters which have been discovered recently by Knudsen effusion-mass spectroscopy [4,6,7]. The common matrix of these systems is the extremely stable Sb tetramer. This unit which has the structure of a regular tetrahedron [9,10] forms by far the most abundant component in the vapor over the intermetallic mixtures studied, as is evidenced by numerous mass spectrometric measurements [11–13]. Both the extraordinary stability of Sb_4 and its tetrahedral symmetry can be linked to the number of 20 valence electrons exhibited by this unit. On the basis of simple skeletal electron pair (SEP) counting rules [14,15], tetrahedral structure is predicted for any homoatomic tetramer with 20 valence electrons. With more refined arguments, derived from a Walsh diagram which displays the relation between molecular orbital energies and cluster symmetry, Cave *et al.* [16] conclude that also in the case of heteroatomic complexes with four constituents and with a valence electron count of 20, tetrahedral symmetry is strongly favored, unless the electronegativity differences between the cluster components are too large.

Experiments in which the gaseous phase over the systems antimony/tin/cesium or antimony/indium/cesium was analyzed [6] have led to the isolation of the cluster species Sb_3SnCs and Sb_3InCs_2, respectively. The former is interpreted as the product of an isoelectronic substitution process

in which one Sb atom is replaced by a SnCs unit. Following the ZKB principle, one expects the Sb_3Sn cluster nucleus of the Sb_3SnCs system to exhibit the same structure as the Sb_4 matrix, i.e., tetrahedral symmetry. The Cs atom should act as an electron donor, transferring ideally one electron which completes a count of 20 valence electrons on the cluster nucleus. However, it is an open question if the amount of charge transfer from the alkali-metal species to the cluster nucleus is sufficient to create a stable 20 valence electron configuration, corresponding to a Sb_3Sn^- ion for which tetrahedral geometry is predicted by the ZKB principle. This problem will be treated in Sec. III of this work by an *ab initio* analysis of the free Sb_3Sn cluster and subsequently of the same system in combination with a Cs atom. By this research, it will be possible to evaluate to what extent the equilibrium structure of the Sb_3Sn species approaches the form of a perfect tetrahedron in the presence of a Cs electron donor.

In the case of the second Sb-based system mentioned above, a cluster of the composition Sb_3InCs_2, the ZKB principle might apply in a more extended sense. Again, one arrives at a number of 20 valence electrons for this unit. However, the Sb_3In cluster nucleus will be stabilized in tetrahedral geometry only if the addition of two Cs atoms gives rise to a very substantial electron transfer. As recent investigations demonstrate, the Zintl concept can be used very successfully to explain the structure of the solid compound Sb_3InCs_2 [4,6]. Nevertheless, it has only been conjectured so far that the same stabilization principle might be operative in the case of the analogous free cluster system. This problem will be discussed in further detail in Sec. III on the basis of an *ab initio* comparison between equilibrium structures and stabilities of the free Sb_3In unit and of the same complex as part of the Sb_3InCs_2 system.

Experimentally, only Cs containing Zintl clusters of the form Sb_3SnA and Sb_3InA_2 (A denotes alkali-metal atom) have been detected so far. Replacing cesium by sodium or potassium in Sb_3SnA or Sb_3InA_2, one anticipates on the basis of electronegativity considerations a weakening of the electron transfer from the alkali-metal species to the cluster nucleus. Thus, using the Zintl concept, both a destablization of the respective cluster and their stronger deviation from the ideal tetrahedral form are predicted for Na and K containing complexes as compared to the Cs containing unit. It is among the purposes of the work presented here to decide if this intuitive expectation can be confirmed by an examination from first principles.

The literature on Zintl systems has been confined for the most part to complexes involving Zintl anions. Formally, one can also construct Zintl cations. In these systems, isoelectronic replacement of a cluster nucleus element leads to the formation of a positively charged cluster nucleus, associated with the presence of additional atoms which act as electron acceptors. In solid and liquid phases, only a few examples for Zintl cations have been found [4,8]. In recent mass spectrometric experiments, however, the first isolation of free clusters which can be characterized as involving Zintl cationic systems has been achieved [6]. Among these newly discovered species are the complexes Sb_3TeBr, Sb_3TeCl, and $Sb_2Te_2Br_2$, which appear to be derived from the Sb_4 matrix. The Zintl cationic systems result from the substitution of one or two atoms by Te units. However, replacement of one Sb atom in Sb_4 by one Te atom requires the addition of a halogen atom for restoration of the original 20 valence electron counts on the cluster nucleus. The Sb_3Te nucleus will consequently acquire positive charge and thus be cationic in nature, weakly bonded to the negative halogen ion which results from the electron transfer process.

Using the ZKB principle as a guideline, one will expect a strong tendency of the Sb_3Te cluster nucleus in $Sb_3TeHalo$ (Halo: halogen atom) to attain tetrahedral equilibrium geometry. As in the examples for Zintl anions introduced above, this feature will depend on the amount of electron transfer between the cluster nucleus and the added atom.

If it can be proved that indeed tetrahedral symmetry of the Sb_3Te cluster nucleus results as a consequence of a sufficiently strong electron subtraction from that unit, an adequate generalization of the ZKB principle has to be proposed which then should embrace the cases of both anionic and cationic cluster nuclei. This assessment requires an accurate description of the main structural and bonding characteristics of the experimentally identified $Sb_3TeHalo$ clusters. Our present investigation tries to provide these pieces of information which have been lacking so far.

Thus, the goal of this study is a clarification of the interrelations between cluster stabilities and geometries as well as electron transfers between different cluster components for the species Sb_3SnA, Sb_3InA_2 (A=Na,K,Cs), and $Sb_3TeHalo$ (Halo=Cl,Br,I). In an earlier investigation [17], we have established a systematic connection between electron transfer to a Sb_4 cluster nucleus and the geometry of this unit for the case of 22-, 24-, and 26-valence electron systems of the form A_nSb_4 (A=Li,Na,K,Cs) [17]. The research reported here is thus a logical continuation of the efforts described in the foregoing article.

The following section will give an outline of the procedure applied in our first-principles calculations. In Sec. III we discuss the individual systems investigated. Section IV adds some concluding comments.

II. PROCEDURE

The present investigation deals with the structure and properties of the Zintl cluster systems Sb_3SnA, Sb_3InA_2 (A =Na,K,Cs), and $Sb_3TeHalo$ (Halo=Cl,Br,I). Moreover, we carry out a study on the pure cluster nuclei Sb_3Sn, Sb_3In, and Sb_3Te, which do not contain any additions of alkali-metal or halogen atoms to enhance our understanding of the Zintl cluster systems.

The discussion which will be given in Sec. III on the crucial features of these units, pertaining to structure, stability, and bonding, is based on information on their equilibrium geometries. We have obtained stable structures for the species involved by performing *ab initio* calculations for each of them. In each individual case, the total cluster energy was minimized as a function of the interatomic distances between all cluster constituents. In these investigations, the Hartree-Fock procedure has been applied in combination with the pseudopotential approach [18]. We employed Gaussian double-zeta basis sets for all systems considered [19–21] and enhanced their flexibilities by adding polarization functions [22].

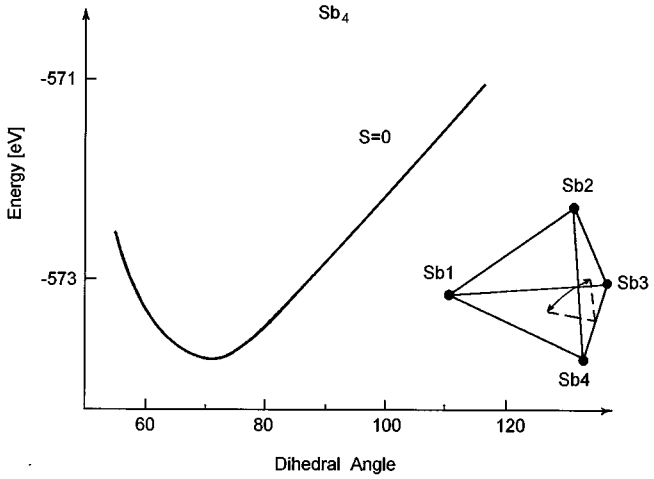

FIG. 1. Minimization curve for Sb_4. The minimum cluster energy is plotted versus the dihedral angle α quoted in degrees. For each value of α considered, a geometry optimization has been carried out.

To ensure the adequacy of this treatment for the description of the Zintl clusters which form the topic of this study, we subjected our method to several tests, dealing first with the pure Sb_4 unit.

Since the emphasis of our investigation is on the structural aspects of Sb-based clusters which originate from Sb_4 by isoelectronic substitution for one Sb atom, a correct representation of the antimony tetramer is an essential criterion for the accuracy of our method. In a first step, we carried out a geometry optimization for the Sb_4 cluster. The energy minimization curve resulting from this preliminary study is displayed in Fig. 1, which shows the total energy of the Sb tetramer versus the dihedral folding angle between two Sb_3 triangles (see inset). For each angle chosen, the cluster energy was minimized as a function of all interatomic distances. The absolute minimum of the curve is found at the geometry of a perfect tetrahedron with an Sb—Sb distance of $D=2.84$ Å, which is in very good agreement with the literature value of $D=2.874$ Å [10]. This latter finding was obtained by a complete active space multiconfiguration treatment followed by multireference configuration interaction (CASMCSCF-MRCI) and hence a considerably more extensive procedure than employed in this work. A geometry optimization in which a second order perturbation treatment for the correlation effect was used yielded a bond distance of $R=2.875$ Å and thus a nearly perfect agreement with the literature value.

In a second examination of the approach used in our investigation on Zintl clusters, we calculated the experimentally known ionization energy of the Sb_4 complex. The experimental value of this quantity is given by Cabaud *et al.* [23] as $\Delta E_{\text{ion}}(\text{Sb}_4)=7.70(0.06)$ eV. Using Koopman's theorem and the orbital energy of the highest occupied molecular level in the optimized Sb_4 structure in Hartree-Fock approximation, we arrive at $\Delta E_{\text{ion}}(\text{Sb}_4)=7.76$ eV, which reflects the experimental finding within its error limits. When a Møller-Plesset perturbation calculation of second order in many-body effect using the available MPL subroutines in the GAUSSIAN92 set of programs was performed for the Sb_4 tetrahedron at optimized bond length and total energies were evaluated for the neutral and singly ionized Sb_4 species, the theoretical result obtained was $\Delta E_{\text{ion}}(\text{Sb}_4)=7.708$ eV, which is in even closer agreement with the mean experimental value.

As outlined in the Introduction, a crucial aspect of the comparison between different cluster systems is that of their respective stabilities, which possibly offers an explanation why certain members of the Zintl cluster group Sb_3SnA, Sb_3InA_2, and $Sb_3TeHalo$ have been spectroscopically identified while others have not. As a measure of cluster stability we use the atomization or stabilization energy of the system, given by the expression

$$\Delta E_{\text{stab}}=3E_{\infty}(\text{Sb})+E_{\infty}(C)+nE_{\infty}(A)-E(\text{Sb}_3CA_n),$$

where C (=In,Sn,Te) denotes the constituent substituted for Sb in Sb_4, A stands for the alkali-metal or halogen constituent added to the Sb_3C cluster nucleus, and n is the number of atoms of the sort A. The symbol $E_{\infty}(X)$ indicates the energy of a cluster component X at infinite separation from any element of the cluster.

Since the stabilization energies for various isomers of any cluster species differ by relatively small amounts, in comparing their stabilities it is important to obtain the differences between these energies as accurately as possible. For that reason, we have evaluated the stabilization energies for the different isomers using both the Hartree-Fock approach as well as one including correlation energies. The latter were computed with the MP2 subroutine of the Gaussian computer programs employed in our work. The ordering of the energies of the various isomers turned out to be the same at both levels of approximation.

However, it is interesting to compare the absolute value of the calculated stabilization energy for the Sb_4 tetrahedron with the experimental finding available for that quantity. The two values are, respectively, 6.19 eV and 8.94 (0.12) eV [23]. While there could be other contributing factors, we believe that the difference between theory and experiment could be reduced through an improved procedure beyond the MP-type correlation treatment used in this work. This treatment is based on a Hartree-Fock V^N potential with only continuum excited states of positive energy. On the other hand, atomic many-body perturbation energy calculations based on the V^{N-1} potential [25] and the corresponding diagrammatic perturbation formalism yield excited states with negative energies, and almost exact agreement with experimental correlation energies is found. This suggests that the use of V^{N-1} potentials in molecular computations together with sizable basis states is the direction for the next step of improvement in the description of many-body effects for molecular systems.

Wherever atomic charges on cluster constituents were considered, the respective values were obtained from a Mulliken population analysis [26] based on the molecular orbital coefficients which resulted from our Møller-Plesset treatment.

Comparison was made between theoretical and experimental ionization energies found from our calculation wherever the latter were available. The measured quantities have to be interpreted as vertical ionization energies [4]. Therefore, in this work, the difference between the total cluster energies at second-order perturbation level for many-body

effects of the neutral and the singly ionized species with the same geometry as the neutral system is expected to represent ΔE_{ion}. Both relaxation and correlation effects of the electronic system are taken into account by this approach.

All calculations reported in the following section have been carried out on the IBM-RISC 6000 computer cluster system of the Cornell National Supercomputer Facility, where use has been made of the program GAUSSIAN92.

III. RESULTS AND DISCUSSION

A. Zintl anions of the form Sb_3SnA (A=Na,K,Cs)

We started our investigation of the Sb_3SnA series by an analysis of Sb_3Sn, the nuclear unit of these clusters. Replacing one of the Sb atoms in the Sb_4 system by a Sn atom, one destroys the tetrahedral symmetry of the Sb_4 cluster. From a geometry optimization in which all interatomic distances of the Sb_3Sn system were varied with respect to each other, we found a somewhat distorted tetrahedron as the equilibrium structure of the Sb_3Sn unit. One could explain these results as follows: Due to a small electronegativity difference between its atomic constituents Sb and Sn, the Sb—Sn bond is more polar than the Sb—Sb bond. Therefore, some electron transfer is seen to occur from Sn to Sb, leading to a positive charge of 0.1 units on the Sn atom and a negative charge of 0.033 units on each of the Sb constituents using the Mulliken approximation [26]. Since this condition gives rise to mutual electrostatic repulsion between the Sb atoms, the Sb—Sn distance contracts and the Sb—Sb distance stretches as compared to the equilibrium bond length of Sb_4, which we determined as D(Sb—Sb)=2.84 Å. For the Sb—Sb distance in the Sb_3Sn cluster, a result of D(Sb—Sb)=2.92 Å is found, for the Sb—Sn distance D(Sb—Sn)=2.81 Å.

It is interesting to note that this calculated geometry and the charges on Sn and Sb lead to an electric dipolar moment of 1.08 D while the calculated dipolar moment including the net contributions from all factors involved is 1.66 D. This finding indicates that the charge-transfer mechanism is a major contributor to the dipole moment.

In order to establish a measure for the deviation from tetrahedral symmetry exhibited by a tetranuclear cluster, we define the quantity R as the ratio between the largest and the smallest interatomic distance present in the cluster system. To compare the degrees of distortion of different structures consisting of four atoms, we will use the expression $R-1$, quoted in percent. On this scale, the perfectly tetrahedral Sb_4 cluster marks the point zero. For Sb_3Sn, we arrive at $R-1=4.15\%$, as shown in Table I. Thus, substitution of a Sn atom for an Sb atom in the Sb_4 unit results in a sizable distortion of the cluster geometry. This structural change is accompanied by a marked destabilization (see Table I). The stabilization energy drops from $\Delta E_{\text{stab}}=6.19$ eV to $\Delta E_{\text{stab}}=5.23$ eV as one goes from Sb_4 to Sb_3Sn.

TABLE I. Stabilization energies, distortion, and charge-transfer parameters for Sb_3Sn and Sb_3SnA (A=Na,K,Cs).

	Minimum energy	Stabilization energy	Asymmetry parameter	Charge on	
A	E_{min} (eV)	E_{stab} (eV)	$R-1$ (%)	A	Sn
		(I) Sb_3Sn			
	527.42	5.23	4.15		0.10
		(II) Sb_3 site variant of Sb_3SnA			
Na	535.46	8.37	0.25	0.40	0.04
K	534.61	8.44	0.91	0.67	0.04
Cs	534.13	9.60	1.33	0.77	0.03
		(III) Sb_3Sn site variant of Sb_3SnA			
Na	535.22	8.14	7.81	0.43	−0.10
K	534.40	8.23	5.79	0.70	−0.19
Cs	533.95	9.43	4.58	0.79	−0.21
		(IV) SbSn site variant of Sb_3SnA			
Na	535.17	8.08	10.92	0.42	−0.11
K	534.29	8.12	8.20	0.69	−0.23
Cs	533.81	9.28	6.16	0.79	−0.26

Should the ZKB principle be valid for Sb_3SnA clusters, one will expect a restoration of the original tetrahedral symmetry when an electron donor in the form of an alkali-metal atom is added to the Sb_3Sn cluster nucleus. Depending on the extent of electron transfer from the alkali-metal atom to the Sb_3Sn system, the latter might acquire a Sb_4-analogous

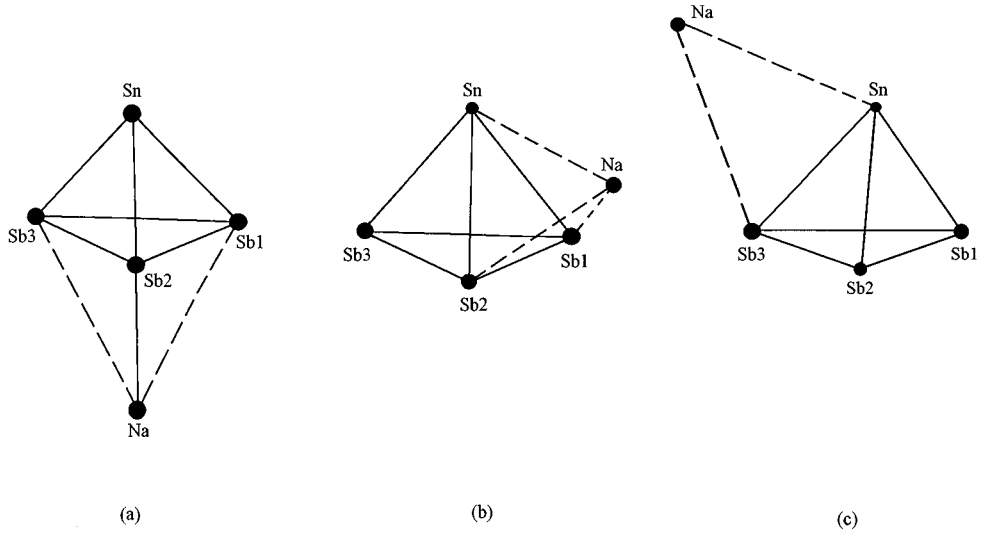

FIG. 2. The three stable structures of Sb_3SnA (A=Na,K,Cs), as discussed in Sec. III A. The species Sb_3SnNa is used as an example: (a) represents the Sb_3 site variant, (b) the Sb_2Sn site variant, and (c) the SbSn site variant.

valence electron configuration and thus approach the structure of a regular tetrahedron.

We examined this expectation by performing geometry optimizations for the systems Sb_3SnA with $A=$Na, K, and Cs. No structural constraints were imposed on the systems. This procedure yielded three stable positions for the alkali-metal atom added to the Sb_3Sn complex, corresponding to two local minima and one global (deepest) energy minimum. The three sites of the alkali-metal constituent are indicated in Figs. 2(a)–2(c). For each geometry, the vibrational frequencies at equilibrium were evaluated. Since this procedure did not yield any imaginary frequencies, we conclude that the three stationary points identified correspond to true minima. The energetically preferred position is realized by an alkali-metal atom located above the Sb-Sb-Sb face of a Sb_3Sn tetrahedron (''Sb_3 site variant''), as shown in Fig. 2(a). The two less favored sites, corresponding to total energies slightly higher than the value from the global energy minimum, are presented in Figs. 2(b) and 2(c). According to our calculation, the alkali-metal atom can occupy a place above a Sb-Sb-Sn face (''Sb-Sb-Sn site variant'') or a place above a Sb-Sn edge (''Sb-Sn site variant''). It should be noted from the minimal cluster energies given in Table I that the three stable structures emerging from our investigation are quite close in minimal cluster energies. The two local minima are separated from each other by an energy difference in the order of only $\Delta E=0.1$ eV, while the global minimum typically differs from the lower local minimum by an amount of $\Delta E=0.2$ eV. As can be seen from the results for the distortion parameter $R-1$ summarized in Table I, the structure corresponding to the global energy minimum exhibits much smaller deviations from tetrahedral symmetry than the two remaining sites. In all three cases examined, the tetrahedral distortion of the energetically preferred cluster structure amounts to far less than 2%. This means a sizable reduction of the degree of distortion found for the pure Sb_3Sn unit. Thus, in clusters of the form Sb_3SnA, bonding conditions seem to be realized, which allow for the closest to perfect tetrahedral structure of the Sb_3Sn cluster nucleus. Replacement of a Sb atom by an atom with an atomic number smaller by one unit (Sn) and simultaneous addition of an alkali-metal atom as an electron donor results in a nearly complete restoration of the original tetrahedral geometry. This finding is in good agreement with the expectation based on the ZKB principle (see Sec. I).

The stabilization energies quoted in Table I and displayed in Fig. 3(a) for the Sb_3SnA complexes rise as one goes from $A=$Na to $A=$Cs, i.e., with increasing electronegativity difference [27] between the cluster nucleus components and the alkali-metal-atom species. The stronger the electron transfer from the alkali-metal constituents to the cluster nucleus and the closer therefore the electronic system of the Sb_3Sn unit comes to the completion of a 20-valence-electron system, the higher the cluster stability. This feature holds for all three variants of the Sb_3SnA system discussed in the present context. In all three cases, the Sb_3SnCs cluster comes out with highest stability.

While this trend is clearly supportive of the electron transfer model which is associated with the Zintl concept, one cannot rule out possible contributions to the stability from other factors. One such factor is the polarizability of the

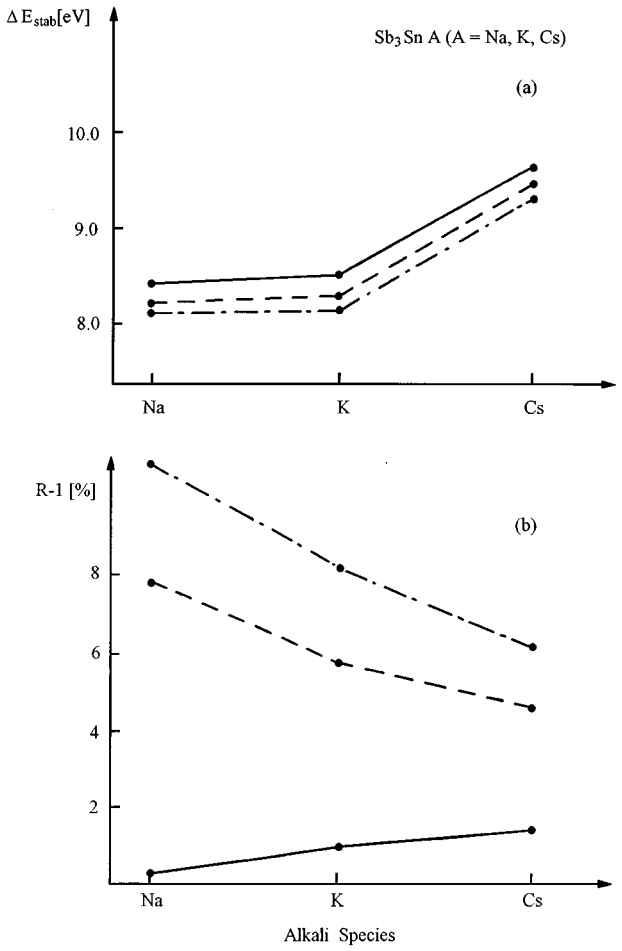

FIG. 3. Stabilization energies and distortion parameters for Sb_3SnA ($A=$Na,K,Cs) versus the alkali-metal-atom species. The lines connecting the points are included for visual clarity. The solid line refers to the Sb_3 site variant [see Fig. 2(a)], the dashed line to the Sb_2Sn site variant [see Fig. 2(b)], and the dot-dashed line to the SbSn site variant [see Fig. 2(c)].

cation component which would lead to a dipole moment on the latter that could add to the stability by its interaction with the cluster nucleus. Both the alkali-metal atoms and the alkali-metal ions exhibit increasing polarizabilities as one goes from lighter to heavier species [29,30]. Since the stabilities of the Zintl systems discussed in the present context increase in the same direction, one might consider the polarizability of the alkali-metal component as one of the factors which determine the stabilities of the Zintl clusters treated in this section.

It must be noted that the energetically preferred cluster variant shows a slight increase in distortion as the electronegativity difference between the alkali-metal species and the remaining cluster components rises. This tendency could be ascribed to a growing polarity of the Sb_3SnA system from $A=$Na to $A=$Cs. The plane of the three Sb atoms separates the alkali-metal atom from the Sn atom which both acquire positive charge. The negative charge concentrated on the three Sb atoms is enhanced from $q(Sb_3)=-0.45$ for Sb_3SnNa to $q(Sb_3)=-0.80$ for Sb_3SnCs. Accordingly, the positive charge of the alkali-metal species grows from q(Na)

TABLE II. Stabilization energies, distortion, and charge-transfer parameters for Sb_3In and Sb_3InA_2 (A = Na,K,Cs).

A	Minimum energy E_{min} (eV)	Stabilization energy E_{stab} (eV)	Asymmetry parameter $R-1$ (%)	Charge on A_1	Charge on A_2	Charge on In
			(I) Sb_3In			
	416.12	4.06	9.02			0.16
			(II) Sb_3InA_2, A_1 on Sb_3 site, A_2 on Sb_2In site			
Na	500.78	8.91	17.34	0.44	0.39	0.02
K	498.92	8.92	15.26	0.67	0.64	−0.09
Cs	497.79	11.08	13.49	0.73	0.73	−0.15
			(III) Sb_3InA_2, A_1 and A_2 on Sb_2In sites			
Na	500.54	8.67	31.70	0.35	0.35	−0.14
K	498.59	8.59	25.83	0.59	0.59	−0.33
Cs	497.48	10.77	19.37	0.72	0.72	−0.42

$=0.40$ to $q(\mathrm{Cs})=0.77$. The increase in electrostatic attraction between Sb_3 and the alkali-metal systems is reflected by a small but steady rise of the distortion parameter from $A=$Na to $A=$Cs.

However, in the other two stable variants of the Sb_3SnA cluster identified by our calculation, we observe the opposite behavior of the cluster distortion as a function of the alkali-metal species. If the alkali-metal atom is located above a Sb_3Sn face or a Sb-Sn edge of the Sb_3Sn nucleus, the deviations from a tetrahedral arrangement of the three Sb atoms and the Sn atom become less as the electron transfer from the alkali-metal atom to the Sb_3Sn complex grows stronger [see Table I and Fig. 3(b)] and the Sb_3Sn cluster therefore approaches a 20-electron situation. This tendency is correlated with the trend of the effective charges concentrated on the nearest-neighbor atoms of the alkali-metal constituent. In the case of both the SbSn site variant and the Sb_2Sn site variant, the atoms closest to the alkali-metal atom are not of the same sort, in contrast to the conditions realized for the Sb_3 site variant. In view of the higher electronegativity of Sb as compared to Sn, the alkali-metal atom transfers more negative charge to the Sb than to the Sn cluster components. This feature introduces a marked asymmetry in the charges of the cluster nucleus constituents, as far as the two energetically less favored variants of the Sb_3SnA unit are concerned. For instance, in the case of the SbSn site variant of the Sb_3SnNa system, we find a charge of -0.11 on the Sn atom while a charge of -0.18 is concentrated on the Sb atom which is closest to the Na electron donor. However, as one goes to the system Sb_3SnCs, the charges are more evenly distributed among the immediate neighbors of the alkali-metal constituent, amounting to -0.27 on the Sn and -0.31 on the Sb atom. As the electron transfer to the cluster nucleus grows stronger, the negative charge is placed more symmetrically, which is reflected by a less marked geometric distortion. Strictly analogous observations can be made for the Sb_2Sn site variant.

From mass spectrometry, the main experimental information about clusters, besides their detected abundance which indicates the stability of the species under examination, is their ionization energy. For Sb_3SnCs, the only system of the form Sb_3SnA experimentally discovered so far [7], the authors report an ionization energy of $\Delta E_{ion}=5.6(0.2)$ eV [7]. This measured datum provides a valuable test of the structural model proposed for the Sb_3SnA series. In view of the time scale of the ionization process involved [4], the vertical ionization potential has to be calculated for a comparison with the experimental finding. In a first approximation, Koopman's theorem might be used for an evaluation of this quantity. This approach describes the ionization energy as the orbital energy of the highest occupied level in the respective system [24]. Adopting this view, we obtain a value of $\Delta E_{ion}=6.05$ eV for the ionization energy of the energetically favored variant of the Sb_3SnCs cluster, i.e., the Sb_3 site variant. This result is already within a range of 10% of the experimental finding, although neither relaxation nor correlation of the electronic system has been taken into account. Making allowance for both these effects by carrying out total-energy calculations including Møller-Plesset perturbation evaluation of second order in the electron-electron correlation effect for the neutral as well as for the singly charged Sb_3SnCs species, we arrive at an improved theoretical value of $\Delta E_{ion}=5.87$ eV, which improves the agreement with the measured result.

B. Zintl anions of the form Sb_3InA_2

In treating this second series of Zintl anions we followed the same procedure as we did in analyzing the Sb_3SnA clusters. In a first step, we investigated the pure cluster nucleus of Sb_3InA_2, i.e., the Sb_3In unit. This 18-electron system deviates more strongly from the very stable 20-electron system Sb_4 than the Sb_3Sn cluster nucleus, involving a 19-electron system. Our geometry optimization yields an equilateral triangle with the length of its side $D=2.99$ Å as the structure of the Sb_3 subunit and a distinctly smaller value of $D=2.74$ Å as the Sb—In distance. The angle $\beta=109.47°$, characteristic of tetrahedral symmetry, is found to be reduced to $\beta=103.49°$. The distortion parameter of Sb_3In (=9.2%, see Table II) is more than twice as large as the distortion parameter found for Sb_3Sn (see Table I). Correspondingly, the cluster stabilization energy exhibits a marked drop as one

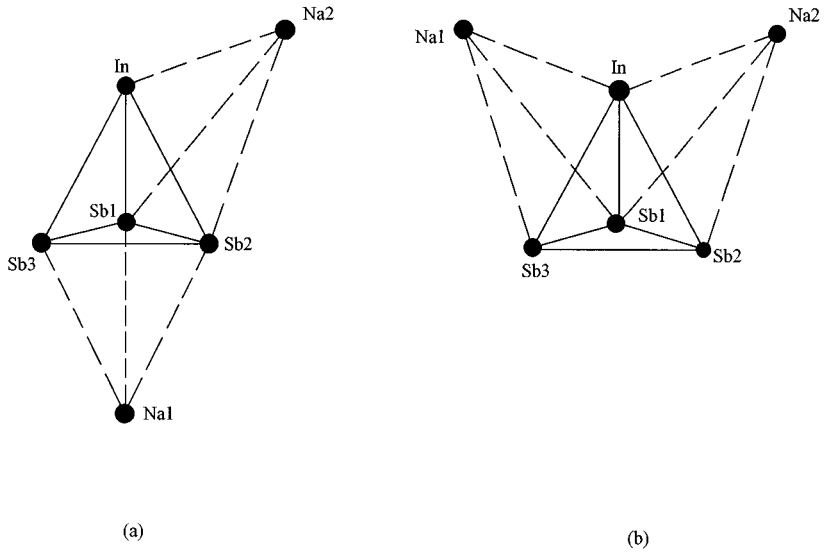

FIG. 4. Two stable structures of Sb_3InA_2 (A = Na,K,Cs), as discussed in Sec. III B. The species Sb_3InNa_2 is used as an example. (a) represents the structural variant with the two alkali-metal atoms placed on inequivalent sites, (b) the variant with both alkali-metal atoms placed on equivalent sites.

goes from Sb_3Sn to Sb_3In (compare the respective values in Tables I and II). In view of the higher electronegativity difference between Sb and In as compared to Sb and Sn, the cluster Sb_3In is characterized by a stronger charge transfer than the cluster Sb_3Sn. This feature accounts for the pronounced differences discussed between the two units.

As two alkali-metal atoms are added which act as electron donors, the 18-electron system could be expected to approach a 20-electron situation. In order to identify the structure of the resulting Sb_3InA_2 cluster, we compared two alternative models. In the first geometric variant, displayed in Fig. 4(a), the two alkali-metal atoms are asymmetrically placed, one facing the Sb-Sb-Sb plane of the Sb_3In cluster nucleus and the other one a Sb-Sb-In plane. The second structure considered is a symmetric arrangement with both alkali-metal atoms located above Sb-Sb-In planes, as shown in Fig. 4(b). In the case of the first model, we determined the structure corresponding to a total-energy minimum by carrying out a geometry optimization in the full 12-dimensional parameter space. The second model examined exhibits higher symmetry than the first. Since the two alkali-metal atoms are situated above equivalent faces of the cluster nucleus, there is invariance of the whole cluster under reflection about a plane defined by the positions of the atoms Sb1 and In as well as the midpoint between Sb2 and Sb3 [see Fig. 4(b)]. This simplification reduces the number of free parameters from 12 to 7. One parameter describes the distance between In and Sb1 and three parameters each give the locations of the atoms Sb2 (Sb3) and $A1$ ($A2$).

Energy minimizations for both structures proposed lead to a preference for the first model, as indicated by the minimum energies given in Table II for both variants of Sb_3InA_2 discussed. The total energies for the two structures at optimized geometries differ consistently by the small amount of $\Delta E \approx 0.3$ eV. Thus, as it turns out from our calculations, the less symmetric of the structural alternatives is energetically favored over the more symmetric one. This feature could be understood in terms of electronegativity differences. Any alkali-metal species differs in electronegativity substantially more from the fifth-group atom Sb than from the third-group atom In [27], which makes the A—Sb bond more polar than the A—In bond. Accordingly, the location above the Sb-Sb-Sb face turns out to be the most stable site of the alkali-metal atom, allowing for its interaction with three neighboring Sb atoms. At the Sb-Sb-In site, in contrast, only two A—Sb bonds can be formed. This crucial difference between both possible positions of the alkali-metal species is reflected by a stronger charge transfer to the cluster nucleus from an alkali-metal atom at the Sb-Sb-Sb site as compared to the Sb-Sb-In site (see Table II). Thus, in accordance with the equilibrium structure obtained for the members of the Sb_3SnA series, we again observe that the Sb-Sb-Sb site of the cluster nucleus is occupied preferentially. On the basis of these findings, it seems evident that the first model considered, with the two alkali-metal atoms situated at inequivalent sites, yields higher stability than the more symmetric second model.

As is seen from Table II, both models proposed lead to sizably larger deviations from tetrahedral symmetry than those found for the less complex Sb_3SnA clusters. This behavior is plausible in view of the fact that the electron transfer from the alkali-metal atoms mainly proceeds to the Sb constituents and much less to the In atom (see Table II). For the more stable of the two Sb_3InNa_2 variants, we observe even a slightly positive charge on the In component, as opposed to much higher negative charges on each of the three Sb atoms. These charges are produced by electron transfer both from the alkali-metal-atom constituents and from the In atom. Due to the considerable charge differences between the In and Sb components of the cluster nucleus, a high degree of distortion of the Sb_3InA_2 species appears plausible. However, the more stable of the two variants proposed exhibits a smaller deviation from tetrahedral symmetry than the less stable one. This tendency is maintained consistently for all clusters of the form Sb_3InA_2 investigated in the present work, in spite of the fact that the first structure [see Fig. 4(a)] is of lower symmetry than the second one [Fig. 4(b)]. As explained above, this less symmetric situation gives rise to a stronger electron transfer to the cluster nucleus, which consequently approaches the 20-valence-electron configuration

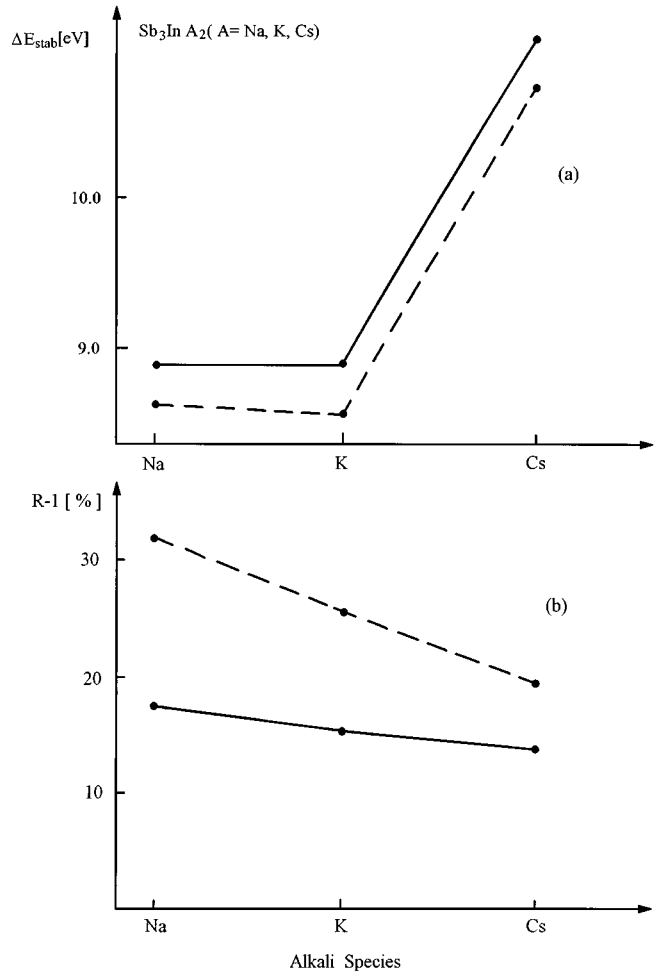

FIG. 5. Stabilization energies and distortion parameters for Sb_3InA_2 (A=Na,K,Cs) versus the alkali-metal-atom species. The lines connecting the points are included for visual clarity. The solid line refers to the first structural variant (the two alkali-metal atoms occupy inequivalent sites), the dashed line refers to the second structural variant (the alkali-metal atoms occupy equivalent sites).

more completely. The stronger charge transfer, associated with the first model proposed, allows for both a more stable and a geometrically more regular cluster nucleus than the second model does.

In Fig. 5, the stabilization energies and distortion parameters of both variants of the Sb_3InA_2 cluster are exhibited as a function of the alkali-metal-atom species. In the case of the first variant, one notes a steady rise of cluster stability as one goes from A=Na to A=Cs, correlated to a steady decrease of the distortion parameter. This behavior is expected considering the increase of electron transfer efficiency in going from Sb_3InNa_2 to Sb_3InCs_2.

The results obtained for the second structural variant of Sb_3InA_2 are not quite as obvious as that of the first. Again, the degree of distortion drops with increasing electron transfer, i.e., from A=Na to A=Cs. This trend, however, is not accompanied by a corresponding enhancement of the cluster stability. For Sb_3InK_2, we find a smaller stabilization energy than for both Sb_3InNa_2 and Sb_3InCs_2. This irregularity could be interpreted as the effect of a competition between the stabilization of the Sb_3In cluster nucleus through electron transfer and a simultaneous destabilization of the cluster by mutual repulsion of the two alkali-metal-atom constituents. This latter interaction causes a continuous widening of the angle included by lines which connect the positions of the two alkali-metal atoms to the centroid of the Sb_3In tetrahedron, as one goes from A=Na to A=Cs. A similar tendency is not found for the more stable cluster variant. In both cluster series compared, however, the Cs containing species is characterized by the highest stability and the least deviation from tetrahedral symmetry.

No ionization energy has been reported so far for the experimentally detected cluster Sb_3InCs_2. On the basis of a Møller-Plesset perturbation treatment of second order in the correlation effect, we predict a value of ΔE_{ion}=4.28 eV. This might be compared to the ionization energy of ΔE_{ion}=5.8 eV calculated for the Sb_3SnCs species (see Table IV) which is close to the mean of the ionization energies of the individual cluster components (ΔE_{ion}(Cs)=3.89 eV, ΔE_{ion}(Sb)=8.64 eV, ΔE_{ion}(Sn)=7.34 eV [28]). For Sb_3InCs_2, in contrast, we arrive at a much smaller result, which indicates that the ionization energy of this species is strongly determined by its Cs constituents.

C. Zintl cation systems of the form $Sb_3TeHalo$

The investigation of the third class of Zintl clusters examined in this work was preceded by an analysis of the pure

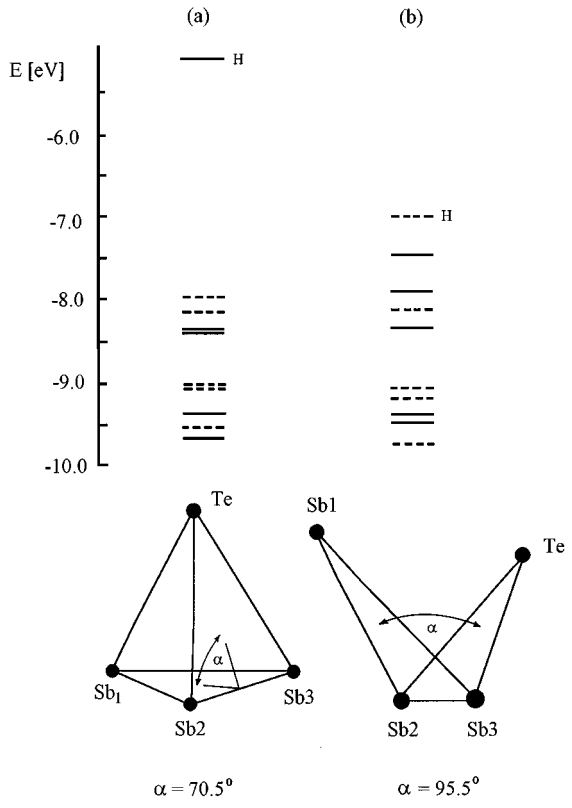

FIG. 6. Sb_3Te cluster in tetrahedral structure (a) and in its equilibrium structure (b) as emerging from a full geometry optimization (see Sec. III C). For both cases, the term scheme for the highest occupied molecular levels is given. Solid lines refer to α orbitals, dashed lines to β orbitals. HOMO and LUMO states are indicated in both cases.

TABLE III. Stabilization energies, distortion, and charge-transfer parameters for Sb_3Te and $Sb_3TeHalo$ (Halo=Cl,Br,I).

Halo	Minimal energy E_{min} (eV)	Stabilization energy E_{stab} (eV)	Dihedral angle	Asymmetry parameter $R-1$ (%)	Charge on Halo	Charge on Te
			(I) Sb_2Te			
	654.08	5.28	95.48	35.60		−0.17
			(II) Sb_3 site variant of $Sb_3TeHalo$			
Cl	1059.41	8.49	92.81	26.07	−0.40	−0.17
Br	1010.76	8.08	93.47	26.71	−0.35	−0.17
I	962.17	7.75	94.10	27.42	−0.29	−0.16
			(III) First Sb_2Te site variant of $Sb_3TeHalo$ (Halo closer to Sb_2 than to Te)			
Cl	1044.95	7.56	65.60	21.41	−0.43	0.03
Br	1009.84	7.17	65.64	21.08	−0.39	0.04
I	961.27	6.85	65.64	20.96	−0.37	0.05
			(IV) Second Sb_2Te site variant of $Sb_2TeHalo$ (Halo closer to Te than to Sb_2)			
Cl	1044.34	7.47	79.12	10.57	−0.48	0.32
Br	1009.83	7.16	78.48	9.70	−0.46	0.27
I	961.34	6.92	78.18	9.25	−0.44	0.21

Sb_3Te unit. In contrast to the Sb_3Sn and Sb_3In systems dealt with in Secs. III A and III B, for the Sb_3Te unit one does not expect the form of a distorted tetrahedron. Instead, a butterflylike structure with wings of different lengths appears more probable [see Fig. 6(b)]. This expectation is based on a Walsh diagram construction for tetratomic systems [16], which represents the expected variation of the orbital energies as a function of the cluster symmetry. According to this scheme, a tetratomic 20-valence-electron system of the form of a regular tetrahedron is characterized by a very sizable HOMO-LUMO gap. Creating a tetrahedral 21-valence-electron system means placing one additional electron in the LUMO state of E symmetry, which is strongly antibonding and much higher in orbital energy than the HOMO state. In this situation, Jahn-Teller distortion results. Corresponding to the two components of a degenerate C_{3v} state, a regular Sb_3Te tetrahedron can distort in two different ways, forming either an acute or obtuse isosceles triangle with a Te atom attached to it. As we find from our study, the former structure is energetically preferred over the latter. Figure 6 displays the Sb_3Te geometry as yielded by our optimization. This cluster deviates strongly from the geometry of the regular tetrahedron, exhibiting a dihedral angle α of 95.5°, as compared to the value 70.5° for the regular tetrahedron. While the energy of the half-filled HOMO state is very strongly reduced, the highest completely filled state is slightly promoted towards a higher energy.

As the term schemes given in Fig. 6 show, the geometry of a perfect tetrahedron corresponds to a HOMO-LUMO gap of $\Delta E = 2.85$ eV, as compared to a much smaller gap of $\Delta E = 0.45$ eV in the case of the equilibrium geometry. Since this geometry resembles a somewhat irregular butterfly structure rather than a deformed tetrahedron, the distortion parameter for Sb_3Te is extremely high, amounting to $R-1 = 35.6\%$ (see Table III). We find for this structure a stabilization energy of $\Delta E_{stab} = 5.28$ eV, which is somewhat higher than the result of $\Delta E_{stab} = 4.36$ eV obtained for the tetrahedral variant of this cluster and also higher than the stabilization energies evaluated for the pure cluster nuclei Sb_3Sn and Sb_3In. Obviously, there are two ways in which the Sb_3Te cluster can be turned into a 20-valence-electron system. It could be singly ionized, or it could be combined with an electron acceptor in the form of a halogen atom. Using the latter possibility, one arrives at the $Sb_3TeHalo$ series which forms the topic of this subsection. The $Sb_3TeHalo$ species can be labeled as Zintl cation systems. These clusters are generated by isoelectronic substitution of a TeHalo unit for a Sb atom in Sb_4. Electron transfer will proceed from the Sb_3Te subunit to the halogen atom thus leaving the cluster nucleus positively charged.

We tested this possibility by performing a full geometry optimization of the system $Sb_3TeHalo$. Using this procedure, three equilibrium configurations of the five atomic constituents were identified, corresponding to a global and two local energy minima. In analogy to the result which we reported in Sec. III A for the Sb_3SnA complex, the global minimum turned out to be associated with a position of the added halogen species above the Sb_3 face of the Sb_3Te cluster nucleus, referred to hereafter as the ''Sb_3 site variant,'' as shown in Fig. 7(a). The two geometries which emerge from our investigations as less stable local minima are illustrated in Figs. 7(b) and 7(c). These two structures have in common that the halogen species is situated above a Sb-Sb-Te face of the Sb_3Te nucleus, in the first case located close to one of the two Sb atoms (''first Sb_2Te site variant''), and in the second case close to the Te atom (''second Sb_2Te site variant''). Vibrational frequency analysis confirmed that these two stationary points indeed are true minima. They are associated with the two components of the degenerate C_{3v} ground state of a tetrahedral Sb_3Te molecule. While in the first of the two isomers the three Sb atoms form an obtuse triangle, in the second isomer, a nearly equilateral Sb_3 triangle is realized. In the following, we will comment first on the properties of the

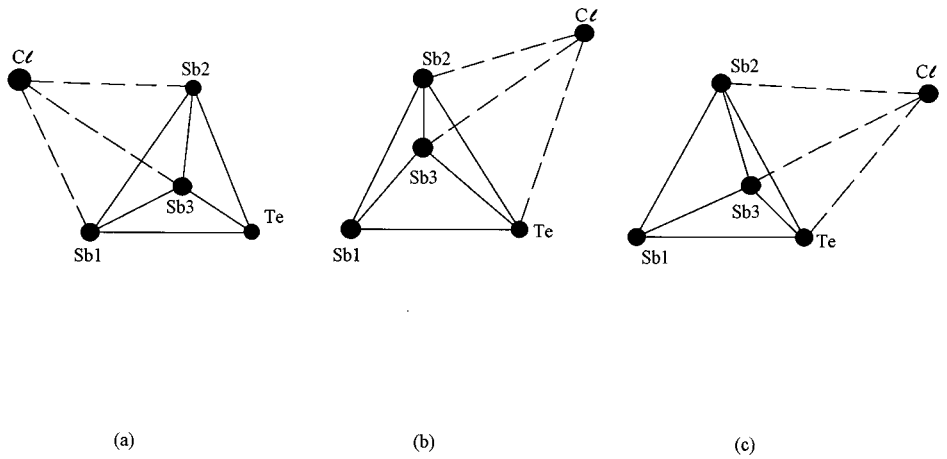

FIG. 7. Three stable structures of $Sb_3TeHalo$ (Halo=I,Br,Cl), as discussed in Sec. III C. The species Sb_3TeCl is used as an example. (a) represents the Sb_3 site variant, (b) the first Sb_2Te site variant, and (c) the second Sb_2Te site variant.

energetically preferred Sb_3 site structure and then on the two remaining ones.

In contrast to the observations made on the Sb_3 site structure of the Sb_3SnA series, we find in the case of the analogous $Sb_3TeHalo$ structure a pronounced asymmetric placement of the electron acceptor added to the Sb_3Te unit. The halogen atom is found at a much closer distance to the ''wingtip'' atom Sb1 [see Fig. 6(a)] than to its other Sb neighbors. This feature is plausible since the Te atom tends to bond mainly with the two ''backbone atoms'' Sb2 and Sb3 and much less with Sb1 which becomes the principal bonding partner for the halogen species. Thus, charge transport proceeds mostly from Sb1 to the halogen atom while the charge of the Te atom remains almost unaffected by the addition of the halogen species, as can be seen from Table III. As our calculation shows, the structure of the free Sb_3Te unit is not markedly changed when the halogen atom is attached to the Sb_3 site. However, the electron subtraction from the cluster nucleus moves it from a pure 21-valence-electron system towards a 20-valence-electron situation. Therefore, one anticipates a smaller degree of distortion for the cluster nucleus of $Sb_3TeHalo$ as compared to the free Sb_3Te cluster, and also a reduction of cluster nucleus distortion as one proceeds from the halogen species—considered in the present context—with lowest electronegativity (Halo=I) to the one with highest electronegativity (Halo=Cl).

Both these expectations are confirmed by our results. The distortion parameter is found to be clearly smaller for $Sb_3TeHalo$ than for Sb_3Te, decreasing from 35.6% to the range of 26%. Also, the values given in Table III (a) indicate that the distortion shrinks as the electronegativity of the halogen species grows, i.e., from Halo=I to Halo=Cl. This trend is also reflected by the behavior of the dihedral angle α which deviates less from the tetrahedral value $\alpha=70.5°$ for stronger electron transfer from the cluster nucleus. In spite of these tendencies it should be pointed out that the overall distortion of the Sb_3Te unit in the energetically preferred structure of $Sb_3TeHalo$ is still quite large. The stability of the $Sb_3TeHalo$ system increases as its nucleus comes closer to the tetrahedral form, i.e., with decreasing distortion parameter.

We find a further reduction of the tetrahedral distortion as we move on to the first Sb_2Te site variant which marks one of the local energy minima. Here again, the halogen atom forms the strongest bond with a Sb atom [labeled ''Sb1'' in Fig. 7(b)], reflected by the sizable positive charge of 0.4 units on the Sb1 atom. However, in contrast to the $Sb_3TeHalo$ geometry discussed above, the halogen species also influences the charge on the Te atom quite drastically, diminishing it from the negative value it attains in the free Sb_3Te unit to the value slightly larger than zero quoted in Table III. Thus the Te atom and the wingtip Sb atom (Sb1) now are both nearly neutral and are therefore expected to have stronger covalent bonding than in case of the Sb_3Te unit where the corresponding bond has more ionic character. This expectation is supported by the decreasing tendency of the Sb1—Te bond length as one goes from Sb_3Te [D(Te—Sb1)=3.79 Å] to the variant of $Sb_3TeHalo$ under consideration [D(Te—Sb1)=2.88 Å]. The Te—Sb1 bond strengthening has a pronounced impact on the $Sb_3TeHalo$ cluster geometry in the first Sb_2Te site variant. As can be seen from Table III, the distortion parameters for this structure are consistently smaller than the ones evaluated for the $Sb_3TeHalo$ structure discussed above and are very sizably decreased as compared to the distortion of the pure Sb_3Te unit. Correspondingly, the dihedral angle between the two wings is strongly reduced from $\alpha=95.5°$ in the pure Sb_3Te unit to $\alpha=65.6°$ in the $Sb_3TeHalo$ variant considered here. This latter value is quite close to the dihedral angle $\alpha=70.5°$ of the perfect tetraheron.

Turning now to the trends in the stability and geometry as functions of the halogen species [see Figs. 8(a) and 8(b)], one notices again an increase of stability with the electronegativity of the halogen component, that is, from Halo=I to Halo=Cl. One might expect to find this tendency reflected by a decrease of the distortion parameter in going from the less to the more electronegative halogen species. In contrast, one notices a very small rise of the distortion parameter from Halo=I to Halo=Cl [see Fig. 8(b)]. We observe a correlation of this behavior with a slight stretching of the equilibrium bond length between Sb1 and Sb2 [see Fig. 7(b)], which is the longest interatomic distance found in the $Sb_3TeHalo$

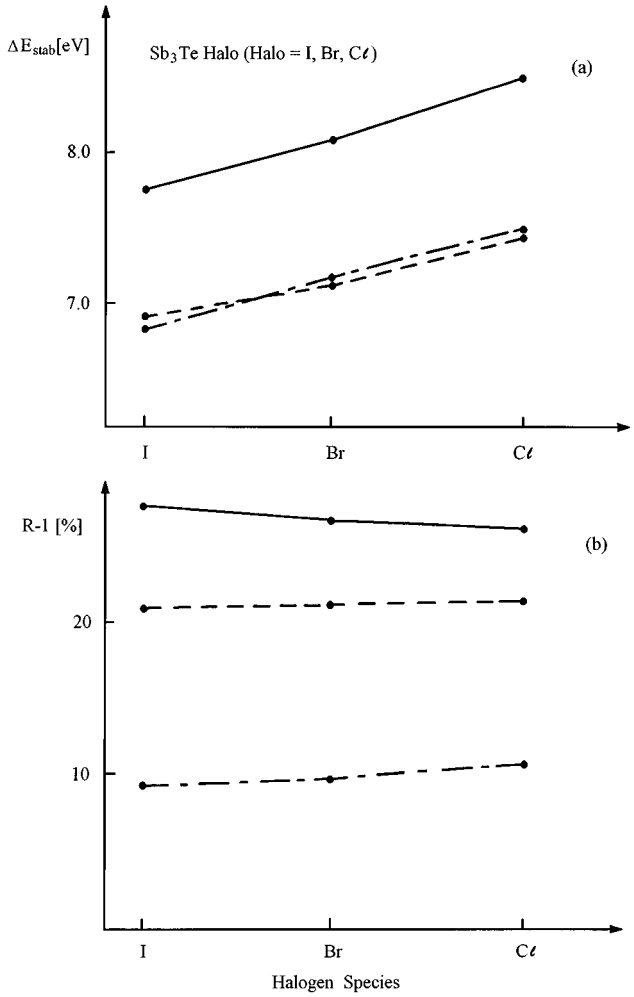

FIG. 8. Stabilization energies and distortion parameters for Sb_3TeHalo (Halo=I,Br,Cl) versus the alkali-metal-atom species. The lines connecting the points are included for visual clarity. The solid line refers to the Sb_3 site variant, the dashed line to the first Sb_2Te site variant, and the dot-dashed line to the second Sb_2Te site variant.

complex (first Sb_2Te site variant). This stretching might be considered to arise from a reduction of covalency of the Sb1—Sb2 bond as one goes from I to Cl. The reason for this reduction is most likely the enhancement of the positive charge on the Sb2 atom through electron donation to the halogen constituent. This positive charge increases from a value of $q(\mathrm{Sb2})=0.30$ for Halo=I to $q(\mathrm{Sb2})=0.42$ for Halo =Cl, which makes the atoms Sb1 and Sb2 increasingly different in nature as one goes from I to Cl and therefore tends to weaken the bonding between them.

Analogous observations are made for the second Sb_2Te site variant of Sb_3TeHalo, which is shown in Fig. 7(c). In this geometry, the halogen atom bonds preferentially with the Te atom. Therefore, the interatomic distance D(Halo-Te) turns out to be much smaller than the distance D(Halo-Sb_i) with $i=1,2,3$. This structure is characterized by the strongest electron transfer from the cluster nucleus to the halogen element in all Sb_3TeHalo variants examined in this work (for a comparison, see Table III). It is therefore not surprising that the distortion parameter is clearly reduced in this second Sb_2Te site variant as compared to the Sb_3 site variant and the first Sb_2Te site variant of Sb_3TeHalo. Both charge transfer and cluster stability increase with the electronegativity of the halogen component.

TABLE IV. Ionization energies ΔE_{ion} for various species. The symbol $\Delta E_{\mathrm{ion}}^{\mathrm{HF}}$ denotes ionization energies calculated on the basis of the Hartree-Fock formalism using Koopmans' theorem. The quantity $\Delta E_{\mathrm{ion}}^{\mathrm{MP2}}$ refers to second-order Møller-Plesset perturbation calculations of correlation energies, and $\Delta E_{\mathrm{ion}}^{\mathrm{expt}}$ stands for ionization energies as experimentally observed.

Species	$\Delta E_{\mathrm{ion}}^{\mathrm{HF}}$ (eV)	$\Delta E_{\mathrm{ion}}^{\mathrm{MP2}}$ (eV)	$\Delta E_{\mathrm{ion}}^{\mathrm{exp}}$ (eV)
Sb_4	7.71	7.76	7.70(0.06)
Sb_3SnCs	5.96	5.87	5.6(0.2)
Sb_3InCs_2	4.28	4.41	
Sb_3TeCl	7.62	7.93	8.0(1.0)
Sb_3TeBr	7.64	7.92	7.8(0.3)

The tendencies of the distortion parameter and dihedral angle α as functions of the halogen species are very similar to those discussed in connection with the first Sb_2Te site variant. Here, however, the angle α results as somewhat larger than the dihedral angle of the regular tetrahedron.

Comparing the three different Sb_3TeHalo variants studied in this work for a fixed halogen species, one notices a clear correlation between the extent of electron transfer and the degree of cluster nucleus distortion, as is obvious from the results given in Table III. The more the Sb_3Te system approaches the 20 electron situation, the smaller the value of the distortion parameter. Thus, the second Sb_2Te site variant of the Sb_3TeHalo system is characterized by both the maximum charge on the halogen electron acceptor and the highest cluster nucleus symmetry.

We conclude our discussion of the Sb_3TeHalo clusters with a comparison between our theoretical considerations and the actual experimental findings. As outlined in Sec. I, only the subspecies Sb_3TeCl and Sb_3TeBr have been detected by mass spectrometric measurement [4,6]. These two clusters come out unambiguously more stable from our calculations than the third cluster investigated, Sb_3TeI. A further test of our model for the Sb_3TeHalo systems is provided by the measured ionization energies of Sb_3TeCl and Sb_3TeBr. As can be seen from Table IV, both values are well explained within the limits of the experimental error by our calculation based on a second-order Møller-Plesset perturbation treatment of the correlation effect. It is a noteworthy aspect of our work on the ionization energies that the orbital energies of the highest occupied states in the respective Sb_3TeHalo systems yield an excellent approximation to the experimental results. This success in the use of Koopmans' theorem in explaining ionization energy results suggests that the contributions of electronic relaxation and correlation to the ionization energies are either both small or nearly cancel each other for Sb_3TeHalo clusters.

IV. CONCLUSION

The observations outlined and discussed in Sec. III enable us to answer, in the framework of the theoretical model

adopted here, the main question treated in this work: To what extent does the Zintl concept apply to free Sb-based clusters of the composition Sb_3SnA, Sb_3InA_2, and $Sb_3TeHalo$? We dealt with this problem by identifying equilibrium geometries for all systems under study and relating the structures obtained to cluster stabilities and to the electron transfer occurring between different cluster components.

In the following paragraphs, we want to summarize the main results which emerge from our *ab initio* investigation of Zintl clusters.

(a) From our work, the applicability of the Zintl concept [2] does not seem to be limited only to condensed matter (solid and liquid) systems, but to apply also to isolated cluster systems, as is shown by the example of the Sb_3SnA (A = Na,K,Cs) cluster series. Isoelectronic substitution of one Sb atom in Sb_4 by the unit SnA yields a nearly tetrahedral Sb_3Sn cluster nucleus. Addition of an alkali-metal atom to the free Sb_3Sn cluster leads to a drastic decrease of its degree of distortion, i.e., its deviation from perfectly tetrahedral symmetry. This result pertains to the most stable of three equilibrium cluster geometries compared to each other in Sec. III A. This preferred structure involves a position of the alkali-metal atom above the Sb_3 face of the Sb_3Sn cluster nucleus (see Fig. 2). The other two possible sites of the alkali-metal species, above a Sb_2Sn face or a SbSn edge, both allow for a sizable charge transfer to the Sb_3Sn unit as well but are associated with an asymmetric placement of the alkali-metal atom. This feature induces a distinctly higher degree of distortion as well as a lower stability in the two geometric alternatives than is found for the energetically favored Sb_3 site structure. Thus, the Sb_3Sn cluster nucleus of the most stable Sb_3SnA structure comes closest to the symmetry of the regular tetrahedron, as compared to the two alternative structures.

(b) An ordering scheme different from the one operative for Zintl anion systems of the form Sb_3SnA emerges from our studies of the Zintl cation systems $Sb_3TeHalo$. Although electron transfer to the cluster nucleus and distortion parameter show the same relation that was observed for Zintl anions, the structure which is closest to tetrahedral symmetry is not the stablest one anymore, as far as cationic systems are concerned. Due to the strongly antibonding nature of the HOMO state in the Sb_3Te cluster, the Sb_4 matrix undergoes a dramatic structural change when one Sb atom is replaced by one Te atom. The resulting geometry, a somewhat asymmetric butterfly shape [see Fig. 6(b)], is very resistant to structural deformations. As a halogen atom is attached to the Sb_3 face of the Sb_3Te cluster, the equilibrium structure of the pure Sb_3Te unit is not substantially affected, and in this way, the stablest variant of the $Sb_3TeHalo$ series is produced. However, as the halogen atom is situated above the Sb_2Te face, the electron transfer increases and the Sb_3Te cluster nucleus now tends towards a more regularly tetrahedral form. The feature that the most stable situation is encountered when the halogen component is located above the Sb_3 face constitutes a clear parallel between the Sb_3SnA and the $Sb_3TeHalo$ cluster groups and thus between Zintl anion and Zintl cation systems. In contrast to the observations made on the Sb_3SnA system, for $Sb_3TeHalo$ the cluster deformation does not shrink with increasing cluster stability, and instead the opposite tendency is observed.

(c) Replacement of one Sb atom in Sb_4 by In requires the addition of two alkali-metal electron donors to reconstitute a 20-valence-electron situation leading to the Sb_3InA_2 species. Both equilibrium geometries identified for the Sb_3In unit in this cluster type [see Figs. 4(a) and 4(b)] exhibit considerably larger degrees of distortion than the pure cluster nucleus Sb_3In. With this argument, it might be questioned if the classification of the Sb_3InA_2 series under the category of Zintl anions is based on an appropriate and well justified use of this term. For both geometric variants of Sb_3InA_2, however, the increase of cluster stability as the alkali-metal species varies from A = Na to A = Cs is accompanied by a marked decrease of cluster deformation. Thus, with the electron transfer to the Sb_3In unit growing in strength, a structural change of this unit towards T_d symmetry is clearly noticeable. Also, the stablest structural variant of Sb_3InA_2 is characterized by the smallest degree of distortion and the highest amount of electron transfer to the cluster nucleus. This feature is very similar for the Sb_3InA_2 clusters and the less complex Sb_3SnA cluster series and thus justifies the characterization of the former as Zintl clusters.

(d) There is experimental support of the results of our theory for the Zintl systems in two respects. Thus, the Zintl anion and Zintl cation systems found to be most stable from our calculations within a particular cluster group coincide with those experimentally isolated. These are Sb_3SnCs, Sb_3InCs_2, Sb_3TeCl, and Sb_3TeBr. Second, for the units Sb_3SnCs, Sb_3TeCl, and Sb_3TeBr, experimental ionization energies are reported. These are well accounted for by our theoretical treatment, both qualitatively by the use of the Koopmans theorem and in more quantitative detail by total-energy calculations for the neutral molecules and the corresponding ions involving the second-order Møller-Plesset perturbation procedure, which includes relaxation and correlation effects occurring in the electronic system.

Our theoretical investigations indicate the validity of the Zintl concept for free Sb_4 analogous clusters. Addition of electron donors in the form of alkali-metal-atom constituents or electron acceptors in the form of halogen atoms to a cluster nucleus leads in all cases considered to a sizable electron transfer between the cluster nucleus and the added atomic species. Furthermore, the structure of the cluster nucleus approaches tetrahedral symmetry as the electron transfer increases in strength. By these observations, it is shown that the validity of the ZKB principle is not restricted to condensed-matter systems and liquids but extends to free clusters as well.

It would be interesting to investigate in the future dimers, trimers, and more complex aggregations of the Zintl systems studied in this work. This extension of our present work could provide a linkage between single Zintl clusters and solid or liquid Zintl phases and thus help in the understanding of the common features that pervade Zintl systems in general.

Further, this work might be extended by explorations of clusters isoelectronic to those investigated here. As is suggested by the Zintl concept and also by some mass spectrometric measurements [3,6], results similar to the ones reported here may be found when Sb is substituted for by another group-V element such as As or Bi. Also, it should be pointed out that both heavier and more complex Sb_4 analo-

gous systems than considered in this study have been recently isolated [4,6]. For instance, the clusters $PbSb_2Te$ and $TlSbTe_2$ or $Sb_2Te_2Br_2$ should be theoretically analyzed to see if they suggest any limitations or modifications of the ZKB principle.

ACKNOWLEDGMENTS

The authors are very grateful to Dr. L. Poth, whose essential contributions to the mass spectrometric exploration of Zintl clusters stimulated this work.

[1] E. Zintl, J. Goubeau, and W. Dullenkopf, Z. Phys. Chem. Abt. A **154**, 1 (1931).
[2] H. Schafer, B. Eisenmann, and W. Muller, Angew. Chem. **12**, 694 (1974).
[3] R. G. Wheeler, K. Lai Hing, W. L. Wilson, J. D. Allen, R. B. King, and M. A. Duncan, J. Am. Chem. Soc. **108**, 8101 (1986).
[4] L. Poth, Ph.D. thesis, Technische Hochschule Darmstadt, Darmstadt, 1994 (unpublished).
[5] R. W. Farley and A. W. Castleman, Jr., J. Chem. Phys. **92**, 1790 (1990).
[6] L. Poth and K. G. Weil, Ber. Bunsenges. Phys. Chem. **96**, 1621 (1992).
[7] A. Hartmann and K. G. Weil, Angew. Chem. Int. Ed. Engl. **27**, 1091 (1988).
[8] H. G. v. Schnering, W. Hanle, and G. Krogull, Z. Naturforschung **34b**, 1678 (1979).
[9] F. Hagelberg, N. Sahoo, T. P. Das, K. G. Weil, and K.-H. Speidel, Phys. Rev. A **46**, 6087 (1992).
[10] H. X. Zhang and K. Balasubramanian, J. Chem. Phys. **97**, 3437 (1992).
[11] K. Sattler, J. Muhlbach, P. Pfau, and E. Recknagel, Phys. Lett. **87A**, 418 (1982).
[12] T. Scheuring and K. G. Weil, Surf. Sci. **156**, 457 (1985).
[13] C. Brechignac, M. Broyer, Ph. Cahuzac, M. de Frutos, P. Labastie, and J. Ph. Roux, Phys. Rev. Lett. **67**, 1222 (1991).
[14] K. J. Wade, Chem. Soc. Chem. Commun. **15**, 792 (1971).
[15] D. M. P. Mingos, Nature **236**, 99 (1972).
[16] R. J. Cave, E. R. Davidson, P. Sautet, E. Canadell, and O. Eisenstein, J. Am. Chem. Soc. **111**, 8105 (1989).
[17] F. Hagelberg, S. Neeser, N. Sahoo, T. P. Das, and K. G. Weil, Phys. Rev. A **50**, 557 (1994).
[18] See, for instance, W. Harrison, *Electronic Structure and the Properties of Solids* (Freeman, San Francisco, 1980), p. 359.
[19] P. J. Hay and W. R. Wadt, J. Chem. Phys. **82**, 270 (1985).
[20] W. R. Wadt and P. J. Hay, J. Chem. Phys. **82**, 284 (1985).
[21] P. J. Hay and W. R. Wadt, J. Chem. Phys. **82**, 299 (1985).
[22] S. Huzinaga *et al.*, *Gaussian Basis Sets for Molecular Calculations* (Elsevier, New York, 1984).
[23] B. Cabaud, A. Horeau, P. Nounou, and R. Uzan, Int. J. Mass. Spectrom. Ion Phys. **11**, 157 (1973).
[24] J. A. Pople, R. Seeger, and R. Krishnan, Int. J. Quantum Chem. Quantum Chem. Symp. **11**, 149 (1977).
[25] T. Lee, N. C. Dutta, and T. P. Das, Phys. Rev. A **4**, 1410 (1971).
[26] R. S. Mulliken, J. Chem. Phys. **36**, 3428 (1962).
[27] See, for instance, J. Moore, *Physical Chemistry* (Prentice Hall, Englewood Cliffs, NJ, 1962), p. 545.
[28] *CRC Handbook of Chemistry and Physics*, 74th ed., edited by D. R. Lide (Chemical Rubber, Cleveland, 1993), pp. 10–207.
[29] H. J. Werner and W. Meyer, Phys. Rev. A **13**, 13 (1976).
[30] P. C. Schmidt, Alarich Weiss, and T. P. Das, Phys. Rev. B **19**, 5525 (1979).